Received: 25 October 2019 | Revised: 17 February 2020 | Accepted: 7 April 2020

DOI: 10.1002/aqc.3357

RESEARCH ARTICLE

WILEY

Application of multiplatform, multispectral remote sensors for mapping intertidal macroalgae: A comparative approach

Thomas Rossiter[1,2] | Thomas Furey[2] | Timothy McCarthy[3] | Dagmar B. Stengel[1]

[1]Botany and Plant Science, School of Natural Sciences and Ryan Institute for Environmental, Marine and Energy Research, National University of Ireland Galway, Galway City, Ireland

[2]INFOMAR, Marine Institute, Rinville, Ireland

[3]National Centre for Geocomputation, National University of Ireland, Maynooth, Ireland

Correspondence
Thomas Rossiter, Botany and Plant Science, School of Natural Sciences and Ryan Institute for Environmental, Marine and Energy Research, National University of Ireland Galway, Galway City, Co. Galway, Ireland.
Email: t.rossiter1@nuigalway.ie

Funding information
Marine Institute, Grant/Award Number: CF/15/02

Abstract

1. Intertidal macroalgal communities are economically and ecologically important and, with a likely increase in anthropogenic pressures, there is need to evaluate and monitor these diverse habitats. Efforts to conserve and sustainably manage these habitats must be underpinned by accurate, cost-effective, and efficient data collection methods. The high spatial and temporal resolution of unmanned aerial vehicles (UAVs), compared with satellites and aircraft, combined with the development of lightweight sensors, provides researchers with a valuable set of tools to research intertidal macroalgal communities.
2. The ability of multispectral sensors, mounted on a satellite, an aircraft, and a UAV, to identify and accurately map the intertidal brown fucoid *Ascophyllum nodosum* (Fucales, Ochrophyta) at a site with a low species diversity of macroalgae were compared.
3. Visual analysis confirmed that the spatial resolution of satellite imagery was too coarse to map intertidal macroalgae as it could not capture the fine spatial patterns of the macroalgal community. High-resolution RGB (colour) imagery, taken during the aircraft and UAV surveys, was used to collect training and reference data through the visual identification and digital delineation of species. Classes were determined based on the level of taxonomic detail that could be observed, with higher levels of taxonomic detail observed in the UAV imagery over the aircraft imagery. Data from both were used to train a maximum-likelihood classifier (MLC).
4. The UAV imagery was able to more accurately classify a distinct *A. nodosum* class, along with other macroalgal and substratum classes (overall accuracy, OA, 92%), than the aerial imagery, which could only identify a lower taxonomic resolution of mixed *A. nodosum* and fucoid class, achieving a lower OA (78.9%). This study has demonstrated that in a coastal site with low macroalgal species diversity, and despite the spectral similarity of macroalgal species, UAV-mounted multispectral sensors proved the most accurate for focused assessments of individual canopy-forming species.

KEYWORDS

Ascophyllum nodosum, intertidal, macroalgae, multispectral, remote sensing, UAVs

1 | INTRODUCTION

Temperate rocky shorelines are typically dominated by dense communities of macroalgal (seaweed) primary producers, providing habitat for a diverse range of other biota (Bruno & Bertness, 2000; Davies, Johnson, & Maggs, 2007; Vadas, Wright, & Beal, 2004). With increasing anthropogenic pressures on intertidal communities (Mineur et al., 2015), an understanding of their distribution and the development of baseline data collection methods is important for their effective conservation and management (Dekker, Byrne, Brando, & Anstee, 2003). Traditional field surveys, although collecting highly detailed and accurate information, are time consuming and restricted in scale (Hennig, Cogan, & Bartsch, 2007; Kerr & Ostrovsky, 2003; Oppelt, Schulze, Bartsch, Doernhoefer, & Eisenhardt, 2012). On the other hand, remote sensing can capture comparatively larger areas, often allowing for standardized, repeat surveys of the same site (Casal, Sánchez-Carnero, Domínguez-Gómez, Kutser, & Freire, 2012), and potentially offering alternative survey methodologies for intertidal data collection.

Traditionally, aircraft have been the dominant remote-sensing platform for macroalgal mapping studies (Bajjouk, Guillaumont, & Populus, 1996; Casal et al., 2012; Dekker et al., 2003; Garono, Simenstad, Robinson, & Ripley, 2004; Oppelt et al., 2012; Stekoll, Deysher, & Hess, 2006), primarily owing to their greater operational flexibility and spatial resolution when compared with satellites (Brodie, Ash, Tittley, & Yesson, 2018). Satellite-based technologies have also been useful for assessing the extent of broad-scale canopy-forming species (Casal, Sánchez-Carnero, Sánchez-Rodríguez, & Freire, 2011; Cavanaugh, Siegel, Kinlan, & Reed, 2010), but for intertidal mapping, the acquisition of satellite images that coincide with suitable tidal and atmospheric conditions (e.g. cloud cover) is challenging (Bell, Cavanaugh, & Siegel, 2015). For temporal monitoring it is important to consider the impact of the variation in tide state during image acquisition. Bell, Allen, Cavanaugh, and Siegel (2020) observed differences in the area of visible kelp canopy at different tidal states, which if not accounted for could lead to erroneous estimates of kelp canopy biomass. The relatively coarse spatial resolution of aircraft has made identification to species level difficult (Cruzan et al., 2016; Oppelt et al., 2012), although success has been achieved with discriminating between spectrally distinct red, green, and brown macroalgal groups (Casal et al., 2012; Hennig et al., 2007) and when mapping homogenous cover species (Dierssen, Chlus, & Russell, 2015; Pe'eri et al., 2008).

The recent and rapid proliferation of affordable unmanned aerial vehicles (UAVs) (Colefax, Butcher, & Kelaher, 2018) has created a promising remote-sensing alternative to aircraft and satellites. UAVs can capture the highest spatial resolution imagery and have the greatest levels of operational flexibility, making them well suited to operating in dynamic environments (Jensen, Hardy, McKee, & Chen, 2011), including the intertidal zone. They are currently the most cost-effective solution over small areas (Matese et al., 2015), with continued technological development and improvements in battery life and payload capacity (Colefax et al., 2018) likely to increase their application for larger areas: for example, some fixed-wing models (Quantum Tron F90+, https://www.quantum-systems.com/project/tron-f90/) can cover up to 7,500 ha (at a flight altitude of 1000 m). UAVs have been successfully used in a wide range of environments including riparian wetlands (Jensen et al., 2011), intertidal seagrass meadows (Duffy, Pratt, Anderson, Land, & Shutler, 2017), intertidal reefs (Murfitt et al., 2017), coastal habitats (Ventura, Bonifazi, Gravina, Belluscio, & Ardizzone, 2018) and wetlands (Doughty & Cavanaugh, 2019). There are now a range of lightweight sensors that can be UAV-mounted (Colomina & Molina, 2014), further increasing their potential applications.

Intertidal macroalgal communities can be spatially and spectrally complex, with species occurring in mixtures over fine scales, requiring high spatial and spectral resolutions to accurately identify the species present. Although hyperspectral sensors have both high spatial and spectral resolutions, they are currently prohibitively expensive (Manfreda et al., 2018), which can act as a barrier to research groups and organizations. It is therefore important to develop remote-sensing methodologies that cover different technologies and budgets. Multispectral sensors typically contain three or more spectral bands (Burns, Berns, & York, 1996), with many current models ranging from five to 12 (Adão et al., 2017). This lower spectral resolution makes them less suited to spectrally complex environments, but they are significantly cheaper and less complex to operate, process and analyse than hyperspectral sensors (Marshall & Thenkabail, 2015). To date, for UAVs, multispectral sensors have primarily been used for precision agriculture, where different band combinations allow for the identification of weeds (Barrero & Perdomo, 2018), the measurement of grass crop quality (Askari, McCarthy, Magee, & Murphy, 2019), and the monitoring of vegetation health, in order to improve yields and harvest efficiency (Candiago, Remondino, De Giglio, Dubbini, & Gattelli, 2015; Kazantsev et al., 2018). Decreasing costs are now seeing them applied to broader environmental questions, with recent uses including the mapping of malaria vector larval habitat (Carrasco-Escobar et al., 2019) and for use in forestry management (Dash, Pearse, & Watt, 2018). Two very recent studies successfully applied UAV-mounted multispectral remote sensing to macroalgal habitats. Taddia, Russo, Lovo, and Pellegrinelli (2019) characterized the presence of submerged green macroalgae, but did not identify the species, and Tait et al. (2019) managed to discriminate between spectrally distinct intertidal species.

Here, the spectral discriminatory ability of multispectral sensors, mounted on a satellite, an airplane, and a UAV, to accurately map the intertidal fucoid *Ascophyllum nodosum* (Ochropyta, Phaeophyceae), a commercially and ecologically important brown macroalgal species common on moderately exposed to sheltered rocky coasts (Stengel & Dring, 1997), was evaluated. An accurate, affordable methodology was developed to support resource management decision making, addressing the following specific challenges:

- How accurately can multispectral sensors map the distribution of *A. nodosum* within a spatially and spectrally complex intertidal environment?

- Which platform(s) achieve the most accurate mapping of *A. nodosum*?
- Can high-resolution RGB imagery be used for the collection of training and validation spectral information?

We provide a novel methodology, presenting details of data collection, processing, and analysis workflows used, and compare the ability of the three remote-sensing platforms to accurately quantify *A. nodosum* distribution.

2 | METHODS

2.1 | Study site

This study was carried out near Béal an Daingin (53°19′19.7″N, 9°37′16.8″W), which lies within the inner reaches of Kilkieran Bay in County Galway, Ireland (Figure 1). The bay itself is characterized by a range of habitats, including, mudflats, coastal lagoons, shallow inlets and bays, reefs, saltmarshes and machair (National Parks and Wildlife Service (NPWS), 2014). The primary underlying bedrock is granite (Könnecker & Keegan, 1983) and the shoreline is dominated by rocky substrate, giving way to muddy sediment in shallow waters (Sides, Picton, Emblow, Morrow, & Costello, 1994). The site is characterized by a relatively narrow intertidal zone, which drops abruptly into muddy sediments, and abuts onto steep granite cliffs, and was chosen for the high abundance of *A. nodosum* and the relatively low species diversity of the canopy-forming macroalgae. Vertical zonation is, in part, controlled by the gentle sloping nature of the intertidal zone, *Pelvetia canaliculata* and *Fucus spiralis* dominate the upper littoral, followed by pure or mixed beds of *A. nodosum* and *Fucus vesiculosus* and, finally, *Fucus serratus* and patchy *Himanthalia elongata* (all Phaeophyceae). There are areas dominated by boulders in the south of the site that support dense, homogeneous patches of *A. nodosum*. Access to the site was provided by a narrow track.

2.2 | Multispectral acquisition

We sought to collect remote-sensing data from the same time of year (June–July), endeavouring to ensure that the three datasets covered the same site (Figure 2). The datasets were collected over a 3-year period, from 2016 to 2018.

2.2.1 | Satellite imagery

The Sentinel-2 satellite mission comprises two polar-orbiting satellites, each mounted with a high-resolution multispectral instrument (MSI). Each MSI can capture 13 bands over a wavelength range of 440–2,200 nm. Four bands had a spatial resolution of 10 m, six had a spatial resolution of 20 m, and three had a spatial resolution of 60 m (Clevers & Gitelson, 2013). Bandwidths range from 15 to 180 nm and are listed in Table S1. A cloud-free Sentinel-2 multispectral image taken on June 16, 2018 at 11:43 GMT was acquired over the Kilkieran Bay area (Figure 2). The timestamp shows that the image was taken approximately 1 hr before low tide (0.7 m), which was at 13:49 GMT, indicating a tide height of approximately 1 m.

2.2.2 | Aerial imagery

An aerial survey was conducted by AirSurvey in July 2016 during clear weather conditions to coincide with low tide at 12:00 GMT (0.8 m), and the survey was planned so that the plane was over Kilkieran Bay approximately 30 min before this time.

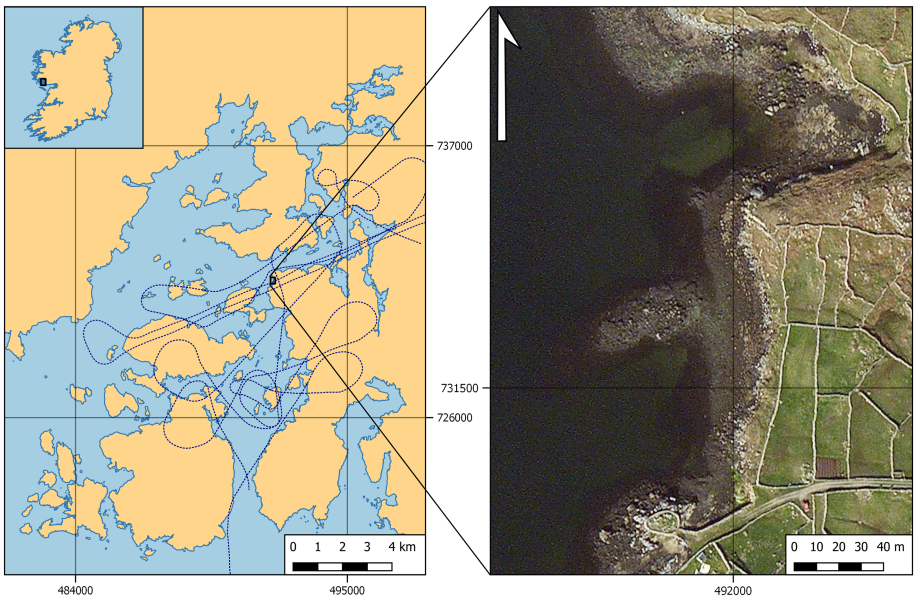

FIGURE 1 Location of the study site at Béal an Daingin in relation to Kilkieran Bay and Ireland. The dotted blue line marks the flight path of the aerial survey. Coordinates are in Irish Transverse Mercator (ITM)

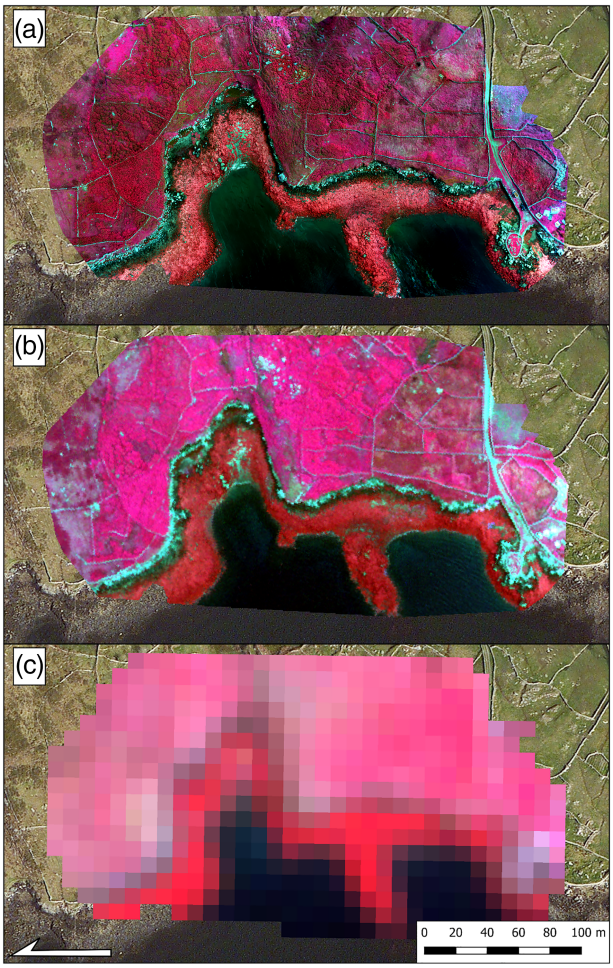

FIGURE 2 Comparison of the multispectral ground sampling distance (GSD) from each of the three platforms: (a) unmanned aerial vehicle (UAV), 5 cm/pixel; (b) aircraft, 60 cm/pixel; and (c) satellite, 10 m/pixel. Layers were clipped to the extent of the UAV imagery

A Cessna-172 (Cessna, Wichita, KS) mounted with an AIRINOV AgroSensor (Parrot SA, Paris, France) was used to collect multispectral data for the intertidal zone in Kilkieran Bay. The sensor, operating as a global shutter, contained four bands: green (550 nm), red (660 nm), red-edge (735 nm), and near-infrared (NIR, 790 nm). The green, red, and NIR bands have a bandwidth of 20 nm and the red-edge is narrower, at 10 nm. There was no integrated light sensor (ILS), so calibration targets were recorded before take-off. Atmospheric conditions were likely to differ over the study area compared with those at the airfield (approximately 135 km away), however, meaning that the radiometric calibration may not be accurate for localized atmospheric conditions. The flight lasted approximately 90 min (not including transit) at an average altitude of 600 m and, providing a ground sampling distance (GSD) of 60 cm/pixel, was tasked with covering as much of the intertidal zone in Kilkieran Bay as possible. A Nikon D800E (Nikon, Tokyo, Japan) camera was mounted on the plane to collect high-resolution RGB imagery (6 cm/pixel). No GPS data were collected for the multispectral imagery and only photo-centre coordinates were available for the RGB (which were not stored in the image tile metadata). The scale of the aircraft survey meant that it was not practical to deploy ground control points (GCPs).

2.2.3 | UAV imagery

A UAV survey was conducted in July 2017 by GeoAeroSpace. Weather conditions were moderately calm and there was significant passing cloud cover. The survey was planned to coincide with the low tide at 12:45 GMT (1 m).

A DJI Inspire V1 (DJI, Shenzhen, China) was used to conduct a multispectral and RGB survey and had a maximum flight time of approximately 18 min, depending on wind speed. RGB imagery was captured using the inbuilt 12 MP X3 camera and a Parrot Sequoia (Parrot SA, Paris, France) sensor was used to collect multispectral data. This four-band sensor records in the green (530 nm), red (660 nm), red-edge (735 nm) and NIR (790 nm) bands, with a 20-nm bandwidth. The Parrot Sequoia operated a global shutter for the multispectral bands allowing the entire scene to be captured simultaneously. There was a separate four-band integrated light sensor (ILS) with an inbuilt GPS sensor. AIRINOV calibration targets were used to calibrate the sensor pre-flight. MAP PILOT 2.7.0 (Drones Made Easy, San Diego, CA) was used to plan the flight. The sensor was not connected to the controller and was set to take an image every 2 s based on an average flight speed of 3 m/s. The UAV flew at an altitude of 50 m, for approximately 12 min, achieving a GSD of 2.2 cm/pixel (RGB) and approximately 5 cm/pixel (multispectral) (Figure 2), and covered a total area of 2.09 ha. Image overlap was set at 70% for RGB and 65% for multispectral (side and frontal) data.

Nine GCPs were deployed to accurately georeference the data. Each GCP consisted of a 50 cm × 50 cm black board with a white cross and a centre point easily visible from the air, the coordinates of the centre point were recorded using a Trimble R8 post-processing kinematic (PPK) global navigation satellite system (GNSS) unit (Trimble, Sunnyvale, CA). GCPs were spaced evenly throughout the site, with one in each corner of the survey area, and the others were spaced to reflect topographical (i.e. vertical) variation. GCPs were post-processed using TRIMBLE BUSINESS CENTRE 5.00 (Trimble, Sunnyvale, CA).

2.3 | Image processing

2.3.1 | Aerial image processing

Aerial RGB imagery was processed using IMAGE COMPOSITE EDITOR (ICE) (Microsoft, Redmond, WA) and ArcGIS 10.3.1 (ESRI, Redlands, CA). The lack of associated GPS data required a more 'manual' approach to data processing. Suitable RGB tiles were mosaicked together in ICE and then manually georeferenced to an ESRI World Imagery basemap in ArcGIS before being re-projected into the Irish Transverse Mercator (ITM) projection. Key identifying features of fixed position, such as wall corners and distinctive rocks, were used to improve accuracy. A single multispectral tile provided sufficient coverage of Béal an

Daingin. After initially being cropped to remove noise, bands were aligned using the AUTO-GEOREFERENCE tool (ArcGIS Pro) and then stacked using the COMPOSITE BANDS tool. The final composite image was then manually georeferenced to the RGB extent and projection.

2.3.2 | UAV image processing

The UAV RGB imagery and multispectral data were processed using PIX4D MAPPER (Pix4D, Lausanne, Switzerland), GCPs were imported, primarily to avoid layer co-registration errors (Bentoutou, Taleb, Kpalma, & Ronsin, 2005), and the calibration targets were imported to calculate reflectance through the empirical line approach (Smith & Milton, 1999). To focus solely on intertidal spectral signatures, the land and water were masked out. The land mask was created manually to remove any terrestrial features and the water mask was created using the normalized difference water index (NDWI), which enhances water features (Xu, 2006) and, using the appropriate threshold (> −0.2), removed most of the water. These were then used to crop the aerial multispectral imagery to the same extent. NDWI is expressed as follows (McFeeters, 1996):

$$\mathrm{NDWI} = \frac{\mathrm{Green} - \mathrm{NIR}}{\mathrm{Green} + \mathrm{NIR}}.$$

The satellite imagery was already georeferenced and as a result of the coarse pixel size no additional processing steps were undertaken for the satellite imagery aside from cropping it to the extent of the aerial and UAV layers.

2.4 | Multispectral classification

2.4.1 | Image-derived training spectra

For the aerial and UAV data, image-derived endmember training spectra were identified using the RGB imagery, as a guiding dataset, with ENVI 5.4 (Harris Geospatial Solutions, Boulder, CO). The usefulness of this approach has been noted by van Iersel, Straatsma, Middelkoop, and Addink (2018) and involves the visual identification of target features (i.e. macroalgal species), using RGB imagery, and then the creation of training polygons around them prior to their spectral information being extracted from the aligned multispectral imagery. Training polygons were created, using the REGION OF INTEREST (ROI) tool, for areas where individual classes were easily observable, and this was easier for the UAV imagery compared with the aerial imagery. The number of training areas per class was dependent upon the observable area of that class, and the area of each polygon depended on the extent of homogenous class cover. Larger classes with more

TABLE 1 Species and features present at sites and the class codes used to represent each for the unmanned aerial vehicle (UAV) and aerial imagery. *Ascophyllum nodosum* was identified as its own class in the UAV imagery ('Asco'), but only a class representing a fucoid mix dominated by *A. nodosum* ('Asco_*Fucus* spp.') was identified in the aerial imagery along with a mixed fucoid class ('*Fucus* spp.'), in which *A. nodosum* was not present. *Himanthalia elongata* was present but not assigned a class owing to low coverage and *Ulva* spp. ('Green') were not classified in the aerial imagery

Species	UAV imagery code	Aerial imagery code	Description
Ascophyllum nodosum	'Asco'	'Asco_*Fucus* spp.'	The 'Asco' class is a pure *A. nodosum* class and 'Asco_*Fucus* spp.' represents a mixed fucoid class dominated by *A. nodosum*
Fucus vesiculosus	'*Fucus* spp.'	'*Fucus* spp./Asco_*Fucus* spp.'	'*Fucus* spp.' is a mixed fucoid class and 'Asco_*Fucus* spp.' represents a mixed fucoid class dominated by *A. nodosum*
Fucus spiralis	'*Fucus* spp.'	'*Fucus* spp./Asco_*Fucus* spp.'	'*Fucus* spp.' is a mixed fucoid class and 'Asco_*Fucus* spp.' represents a mixed fucoid class dominated by *A. nodosum*
Fucus serratus	'*Fucus* spp.'	'*Fucus* spp./Asco_*Fucus* spp.'	'*Fucus* spp.' is a mixed fucoid class and 'Asco_*Fucus* spp.' represents a mixed fucoid class dominated by *A. nodosum*
Pelvetia canaliculata	'*Fucus* spp.'	'*Fucus* spp./Asco_*Fucus* spp.'	'*Fucus* spp.' is a mixed fucoid class and 'Asco_*Fucus* spp.' represents a mixed fucoid class dominated by *A. nodosum*
Ulva spp.	'Green'	–	'Green' is a class comprised of unidentified green macroalgal species
Himanthalia elongata	–	–	–
Decaying macroalgae	'Wrack'	'Wrack'	'Wrack' is a mixture of unidentified decaying macroalgal species in varying stages of decomposition
Substratum	'Substratum'	'Substratum'	'Substratum' represents a mixture of non-vegetated surfaces, such as rock and sediment

homogenous cover required larger, more numerous training polygons. Species present at the site and the class codes used to represent them are highlighted in Table 1. *Ascophyllum nodosum* was easily identifiable in the UAV imagery owing to its distinctive bright coloration and morphology (Figure 3). Where *A. nodosum* was a distinct class for the UAV data, for the aerial data it was not possible to distinguish homogenous *A. nodosum* stands from those mixed with other fucoids, so a combined class was created (Figure 4). For both UAV-derived and aerial datasets, *F. vesiculosus*, *F. serratus*, and *F. spiralis* were combined into a single category ('*Fucus* spp.'). The shrubby nature of the three species leads to a mottled, darker appearance and it was difficult to confidently differentiate them (Figures 3 and 4). *Pelvetia canaliculata* was also incorporated into this class as it occurred infrequently in small patches, making it very difficult to observe in the RGB imagery, and its inclusion as a separate class could have increased classification error as a result of the spectral similarity between brown macroalgal species (Kotta, Remm, Vahtmäe, Kutser, & Orav-Kotta, 2014). Macroalgae wrack (decaying seaweed) was observable in both sets of imagery, but the coarse resolution of the aerial imagery made it difficult to create an accurate training area and, when its inclusion was tested, wrack was extensively overclassified (Figure S1). Small patches of unidentified green macroalgal ('Green') species were present in both datasets yet, again, the coarse resolution of the aerial imagery made it difficult to accurately create training polygons. 'Green' was overclassified when included in the initial UAV imagery classification workflow (Figure S2), and it was decided to exclude it from the final output. Red macroalgae, although present, were also not included as they were almost exclusively situated subcanopy and remote sensing would not have been able to accurately determine their true extent. The spectral properties of rock, mixed sediment, and sand are relatively similar to one another, and sufficiently distinct from macroalgae, that they are combined into their own class.

The spectral separability of endmember classes was determined prior to running a supervised classification algorithm. The mathematical separability of the classes is performed to assess whether sufficient and representative training data have been selected (Richards &

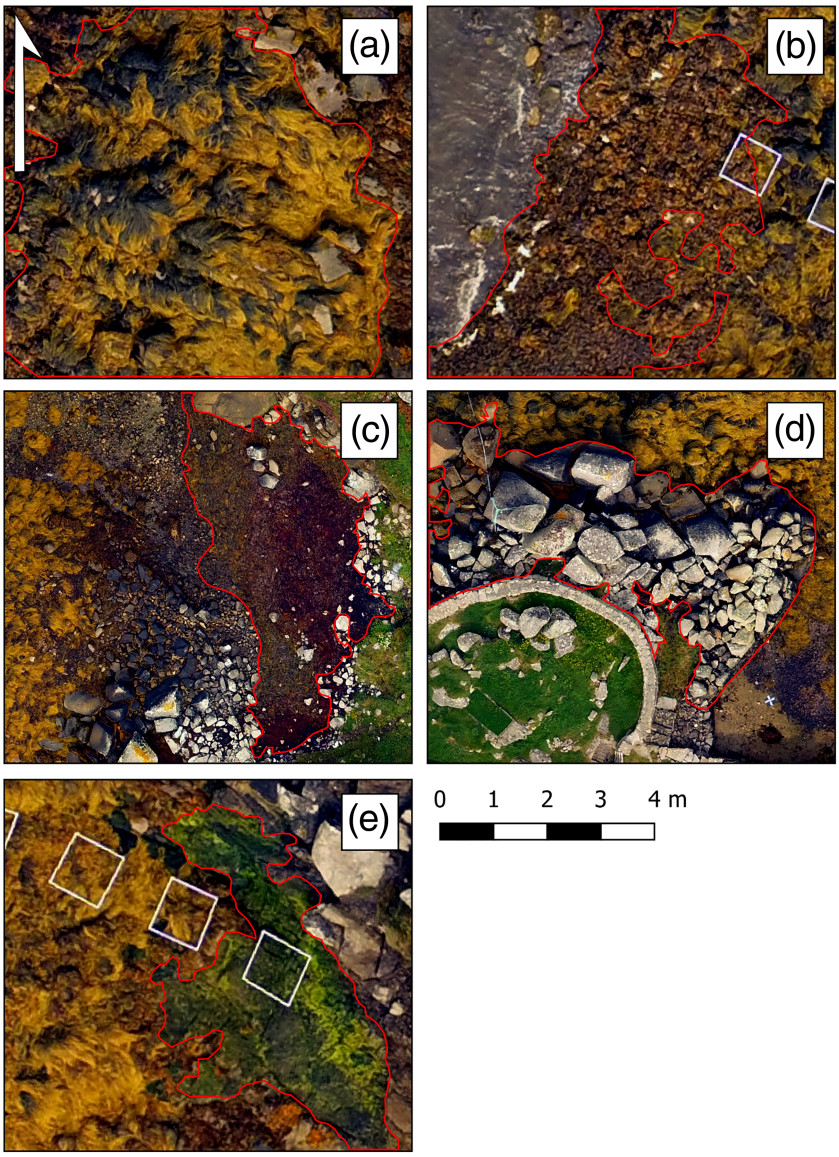

FIGURE 3 Classification classes (highlighted in red) identifiable using high-resolution RGB imagery obtained with an unmanned aerial vehicle (UAV): (a) *Ascophyllum nodosum*; (b) *Fucus* spp.; (c) decaying macroalgae; (d) substratum; and (e) unidentified green species. The distinctive morphological properties of each species were used for the identification

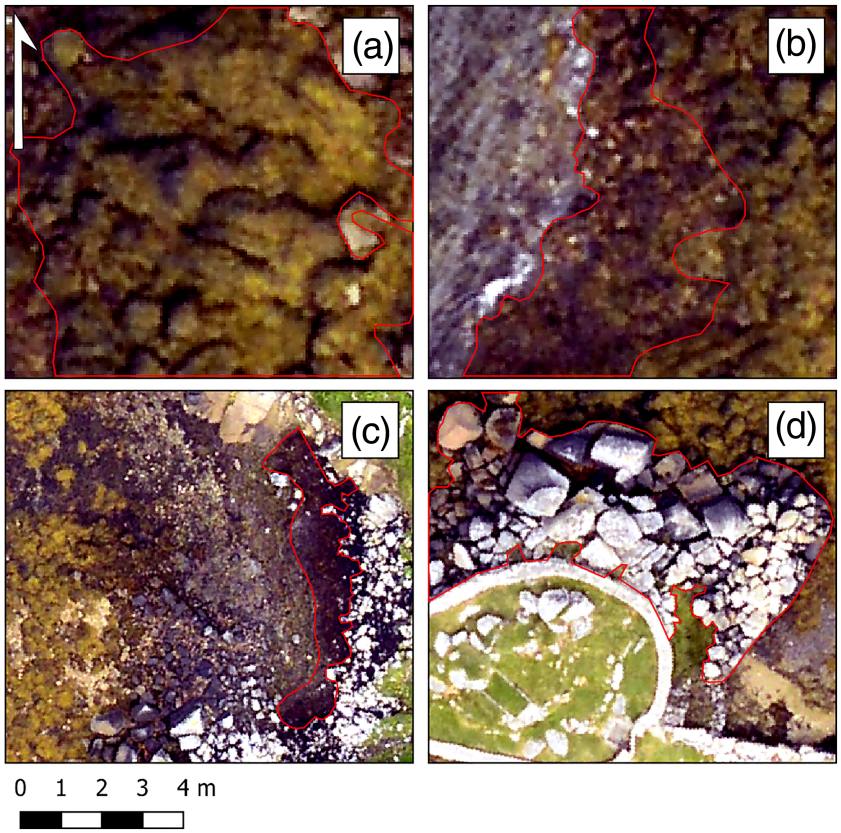

FIGURE 4 Classification classes identifiable using aerial RGB imagery (highlighted in red): (a) mixed *Ascophyllum nodosum* and *Fucus* spp.; (b) *Fucus* spp.; (c) decaying macroalgae; and (d) substratum. Variations in canopy pattern and colour were used for the identification

Jia, 2006). Training data were checked for class separability using the Jeffries–Matusita distance (Jacobsen, Nielsen, Ejrnaes, & Groom, 1999). The values of the resulting output between each pair of classes range from 0 to 2, with 2 indicating perfect separability between them (Richards & Jia, 2006). Good class separability would indicate that sufficient training areas had been selected, whereas lower values would indicate either the need for more training areas or that two classes were inherently similar in their spectral properties. This could then indicate that the two classes could potentially be combined (Petropoulos, Vadrevu, Xanthopoulos, Karantounias, & Scholze, 2010). Despite excluding 'Green' from the final classification, it was included in the spectral separability workflow (UAV imagery) in order to better understand its poor classification performance.

2.4.2 | Supervised classification workflow

For both UAV and aerial multispectral datasets, the supervised classification method of maximum-likelihood classification (MLC) was used in ENVI 5.4. MLC is a popular classifier (Paola & Schowengerdt, 1995) calculating the probability that an individual pixel belongs to a specific class and is based on an estimated probability density function derived from the defined reference classes (Foody, Campbell, Trodd, & Wood, 1992). The MLC classifier assumes a Gaussian distribution for each of the inputted training classes (Jia & Richards, 1994) and can be expressed by the following equation:

$$g_i(x) = \ln p(\omega_i) - \frac{1}{2}\ln|\Sigma_i| - \frac{1}{2}(x-m_i)t\Sigma_i^{-1}(x-m_i)$$

Where i is the class, x represents n-dimensional data, $p(\omega_i)$ is the probability that class ω_i occurs in the image, and is assumed to be the same for all classes, $|\sum_i|$ is the determinant of the covariance matrix of the data in class ω_i, Σ_i^{-1} is the inverse matrix, and m_i is the mean vector.

Maximum-likelihood classification (MLC) was used to classify the training area spectra. No thresholds were selected so that all pixels would be classified, and the spectral separability results were used to determine whether sufficient training areas had been selected so as to be representative of the features present at the site (Richards & Jia, 2006).

2.4.3 | Accuracy assessment

Ground-truth, or reference, data were derived from the high-resolution RGB imagery using the same rationale as for the training data collection. The accuracy of this approach was highlighted by Lechner, Fletcher, Johansen, and Erskine (2012) and it was also found to be more reliable and accurate than GPS-based validation methods (Laliberte & Rango, 2011). Reference data collected from *in-situ* field observations are considered the most accurate, but this can be time consuming, meaning that data derived from imagery are more common (McDermid, Franklin, & LeDrew, 2005; McRoberts et al., 2018).

Polygons were selected for each of the four UAV and three aerial classes, and this was carried out independently of those used to create the training areas in ENVI 5.4. Polygons were created so that they covered as much of each class as possible and only in areas where homogeneous class coverage could be confidently identified. The accuracy assessment tool was used to create the confusion matrix and derive quantitative measures of accuracy (kappa, user/producer accuracy (UA/PA), and errors of commission/omission).

3 | RESULTS

3.1 | UAV classification results

Classification results for the UAV imagery showed the mid-intertidal zone to be dominated by dense beds of *A. nodosum*, with narrow bands of mixed fucoid assemblages dominating in the upper (*F. vesiculosus*, *F. spiralis*, and *P. canaliculata*) and lower (*F. vesiculosus* and *F. serratus*) zones. Decaying macroalgae was present in patches in the extreme upper intertidal zone, and this was most notable in the north-east corner of the site (Figure 5).

Spectral separability results show good separation between all classes with all pairs, apart from 'Asco' and '*Fucus* spp.' (1.7) and 'Green' and *Fucus* spp.' (1.86), having values greater than 1.9, indicating an almost perfect class separation (Richards & Jia, 2006). The slightly lower value for 'Asco' and '*Fucus* spp.' separability highlights their spectral similarities. MLC resulted in an overall classification accuracy of 92% and a kappa coefficient of 0.8733. All four classes showed high user/producer accuracies although, predictably, there is a small amount of misclassification between '*Fucus* spp.' and 'Asco', and also of 'Wrack' as '*Fucus* spp.' (Tables 2 and 3). The misclassification of 'Asco' as '*Fucus* spp.' is spread throughout the site in small patches, whereas the opposite occurs almost entirely in one area (Figure 6). A small area of grass not removed by the land mask was

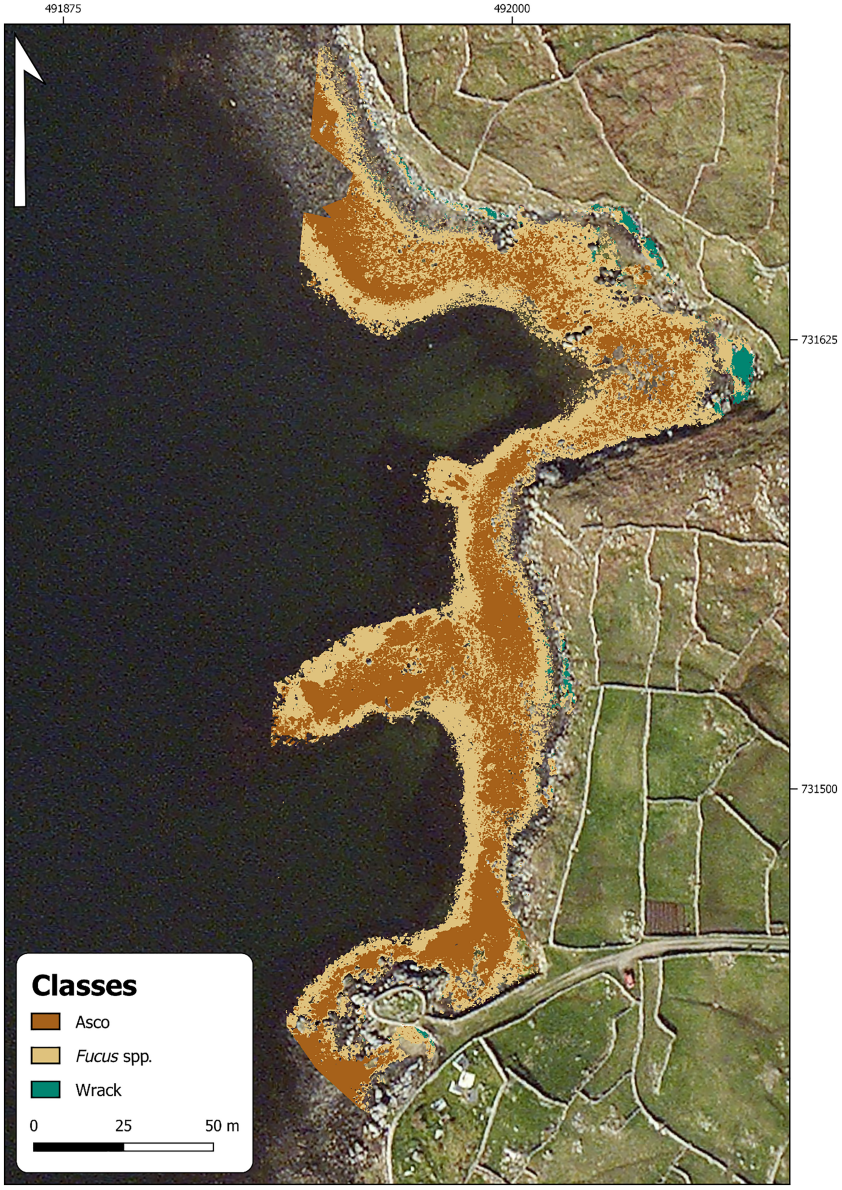

FIGURE 5 Maximum-likelihood classification (MLC) result from the multispectral survey carried out by unmanned aerial vehicle (UAV). Three macroalgal cover classes are displayed over Bing satellite imagery. 'Substratum' was not included. Class codes represent the following species: 'Asco', *Ascophyllum nodosum*; '*Fucus* spp.', mixed fucoids; 'Wrack', decaying macroalgae. Coordinates are in Irish Transverse Mercator (ITM)

TABLE 2 Unmanned aerial vehicle (UAV) multispectral maximum-likelihood classification (MLC) confusion matrix, calculated using ENVI 5.4, by comparing pixels of known class locations with those predicted by the classification workflow, for each of the four cover classes. Results are recorded as percentage of pixels assigned, correctly or incorrectly, to each class

Class	'Substratum'	'Wrack'	'*Fucus* spp.'	'Asco'	Total
'Unclassified'	6.54	0.65	0.03	0.00	1.16
'Substratum'	**91.96**	2.25	0.82	0.01	16.22
'Wrack'	0.08	**91.48**	0.05	0.00	2.48
'*Fucus* spp.'	1.33	5.34	**93.63**	8.83	31.52
'Asco'	0.08	0.00	5.47	**91.16**	48.63
Total	100	100	100	100	**100**

TABLE 3 Unmanned aerial vehicle (UAV) multispectral maximum-likelihood classifier (MLC) user accuracy (UA, probability of correct class assignment, calculated by dividing the number of correctly classified pixels by the total number of pixels in a class) and producer accuracy (PA, correctly classified reference pixels, calculated by dividing the number of correctly classified pixels by the total number of pixels that should be in a class) accuracies for each of the four cover classes, computed using ENVI 5.4

Class	PA (%)	UA (%)	PA (pixels)	UA (pixels)
'Substratum'	91.96	98.12	202,760/220,482	202,760/206,655
'Wrack'	91.48	98.86	31,193/34,100	31,193/31,552
'*Fucus* spp.'	93.63	84.35	338,811/361,862	338,811/401,660
'Asco'	91.16	96.78	599,732/657,877	599,732/619,692

classified as '*Fucus* spp.' in the northern section of the site. 'Asco' covered a total area of approximately 4,127 m^2, out of a total classified area of approximately 12,400 m^2.

3.2 | Aerial classification results

Aerial multispectral classification results revealed a dense covering of mixed fucoid assemblage (*A. nodosum*, *F. serratus*, and *F. vesiculosus*), dominated by *A. nodosum*, in the mid-intertidal zone. Mixed fucoids dominate the upper (*F. spiralis*, *F. vesiculosus*, and *P. canaliculata*) and mid-to-lower (*F. serratus* and *F. vesiculosus*, respectively) intertidal zones (Figure 7).

There was poor spectral separability between 'Asco_*Fucus* spp.' and '*Fucus* spp.' (1.11), but both classes achieved good separation from 'Substratum' (>1.9). These two classes were retained and not combined as their poor spectral separability reflects their inherent spectral similarity. For the aerial imagery there was an overall classification accuracy of 78.9% and a kappa coefficient of 0.6373. 'Substratum' had a high user/producer accuracy, but there was significant misclassification of '*Fucus* spp.' as 'Asco_*Fucus* spp.', resulting in a low producer/user accuracy for '*Fucus* spp.' and a low user accuracy for 'Asco_*Fucus* spp.' (Tables 4 and 5). This misclassification was spread throughout the entire zone dominated by '*Fucus* spp.' (Figure 8). 'Asco_*Fucus* spp.' covered a total area of approximately 5,342 m^2 out of a total classified area of approximately 12,000 m^2.

3.3 | Satellite imagery

The coarse spatial resolution of the Sentinel-2 satellite imagery meant that it was not possible to identify any intertidal macroalgal species to use as training data for a supervised classification workflow. It was, however, possible to visually identify and separate the macroalgae-dominated intertidal zone, covering approximately 8,000 m^2, from terrestrial vegetation and rock/manmade features.

4 | DISCUSSION

The increasing affordability of remote sensing technologies (Colefax et al., 2018) will support their application for a diverse range of ecological monitoring initiatives. The high spatial and spectral resolutions required for the accurate classification of intertidal macroalgal communities (Dekker et al., 2003) can often be expensive (i.e. hyperspectral imaging), acting as a barrier to organizations and research groups. Here, the effectiveness of relatively low-cost multispectral sensors and their platform-dependent spatial resolutions for mapping the distribution of *A. nodosum* was explored. Of the three platforms used, UAV-mounted multispectral remote sensing provided the most accurate results.

The UAV imagery accurately identified and classified a homogenous *A. nodosum* class ('Asco'), distinguishing it from surrounding mixed fucoid assemblages and from base substratum. The high spatial

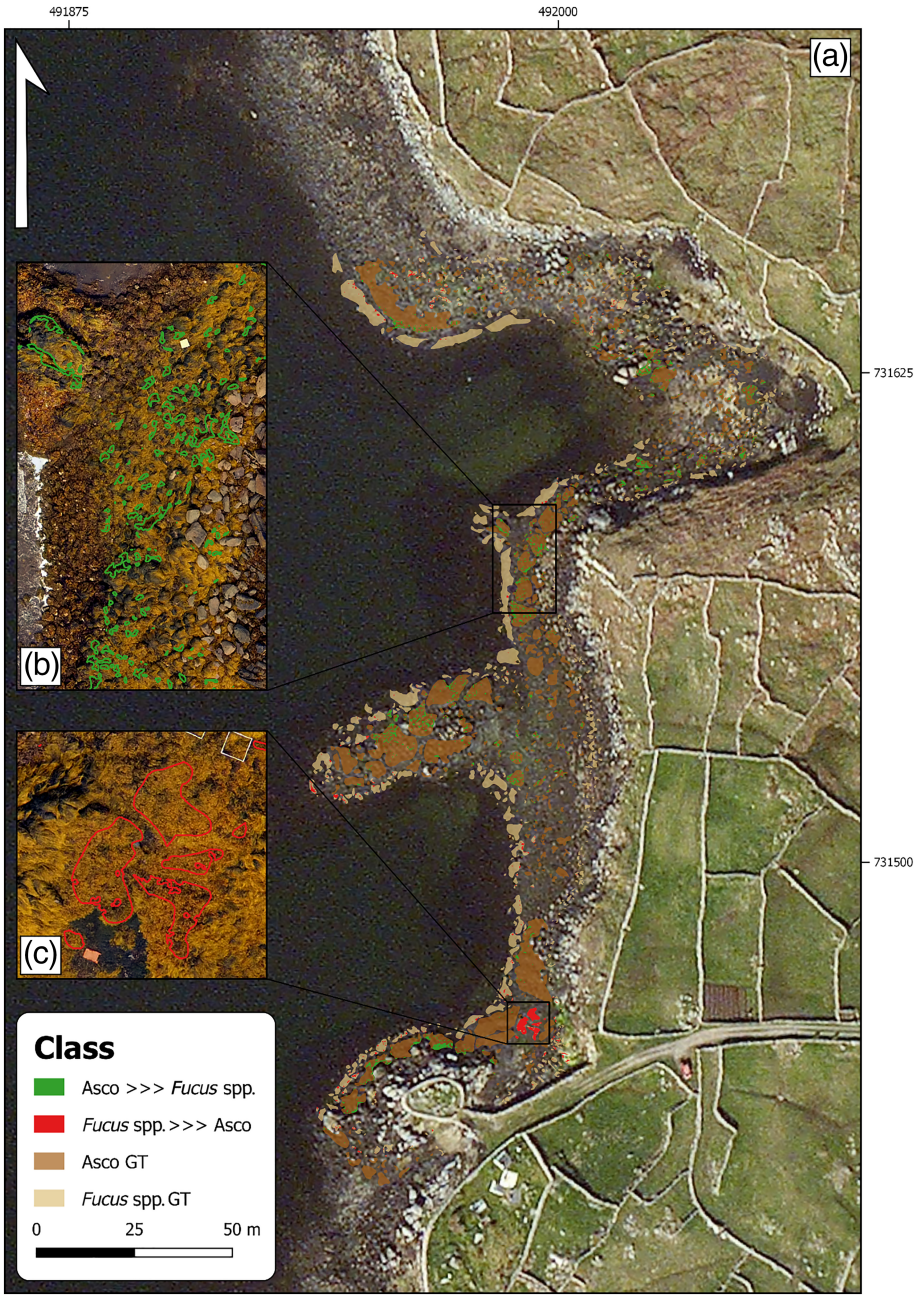

FIGURE 6 (a) Instances of misclassification between 'Asco' and '*Fucus* spp.' displayed above the respective ground-truth (GT) polygons for each class. Insets focus on notable misclassified areas where, in green, 'Asco' has been misclassified as '*Fucus* spp.' (b), and where, in red, the opposite occurs (c). Coordinates are in Irish Transverse Mercator (ITM)

resolution of concurrently collected RGB data allowed for the visual identification of *A. nodosum*, which was characterized by its distinctive morphology and coloration. Despite their inherent spectral similarities (Kotta et al., 2014) and the low spectral resolution of the sensor, clear separation between the macroalgal classes could be achieved. Coarser-resolution aerial imagery was able to classify a lower taxonomic resolution of mixed *A. nodosum* and *Fucus* spp. ('Asco_*Fucus* spp.'). By contrast, freely available Sentinel-2 imagery was found to be too coarse for mapping intertidal macroalgal communities, as it was not possible to observe the fine-scale assemblages, but it was possible to identify the macroalgal-dominated intertidal zone. Higher spatial resolutions (UAV RGB = 2.2 cm/pixel; aerial RGB = 6 cm/pixel) enhanced not only our ability to visually identify species for training and reference data (Meddens, Hicke, & Vierling, 2011), but also the ability of MLC to assign pixels to classes as because of their smaller size there was less within-pixel spectral mixing (Doughty & Cavanaugh, 2019). In areas with a relatively low diversity of intertidal macroalgal species but with dense, homogenous stands, our results demonstrate that multispectral sensors provided an effective tool for species mapping and a lower cost alternative to hyperspectral sensors.

4.1 | UAV multispectral imagery

Ascophyllum nodosum ('Asco') was accurately identified using the UAV platform (PA = 91%, UA = 96.8%), and the spectral differences

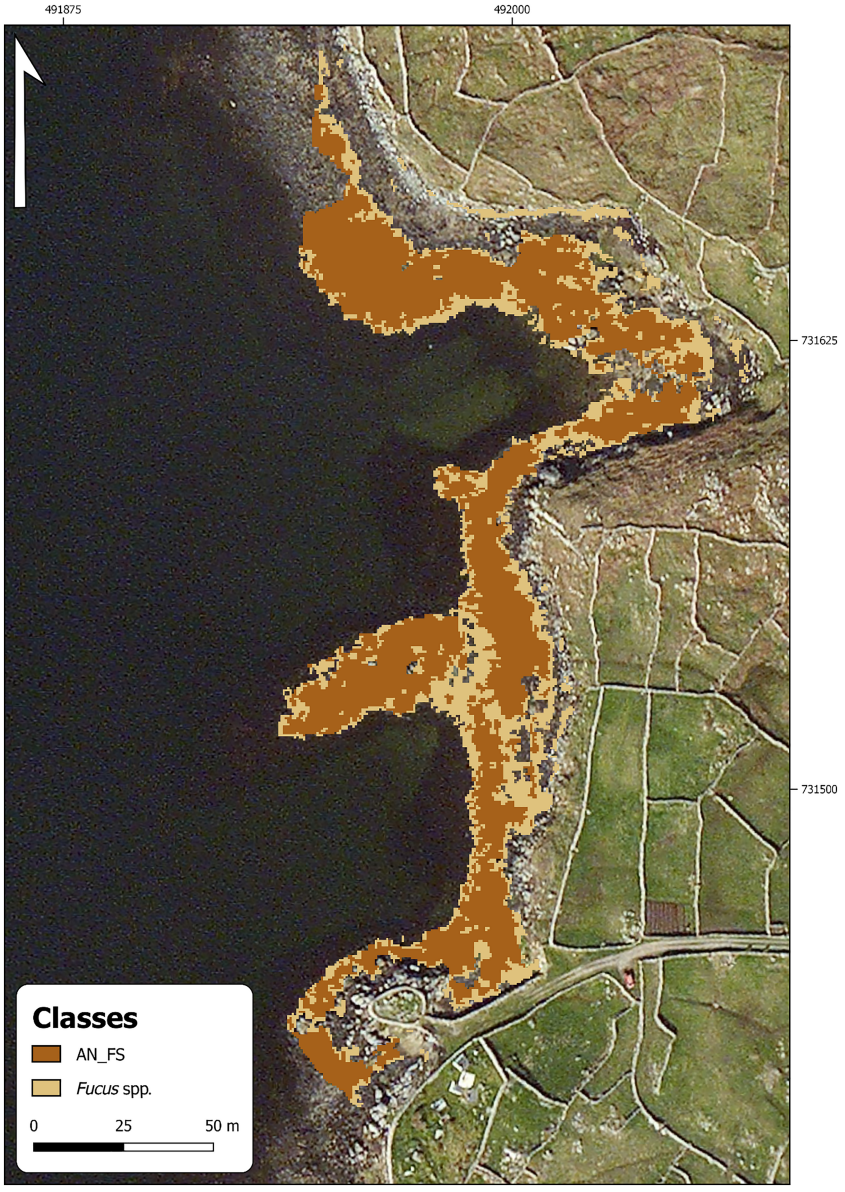

FIGURE 7 Maximum-likelihood classification (MLC) result from the multispectral aerial survey. Two macroalgal cover classes are displayed over Bing satellite imagery. 'Substratum' was not included. Class codes represent the following species: fucoid mix dominated by *Ascophyllum nodosum* (abbreviated here to AN_FS and referred to in the text as 'Asco_*Fucus* spp.') and mixed fucoids ('*Fucus* spp.'). Coordinates are in Irish Transverse Mercator (ITM)

TABLE 4 Aerial multispectral maximum-likelihood classification (MLC) confusion matrix, calculated, using ENVI 5.4, by comparing pixels of known class locations with those predicted by the classification workflow, for each of the three cover classes. Results are recorded as the percentage of pixels assigned, correctly or incorrectly, to each class

Class	'Substratum'	'*Fucus* spp.'	'Asco_*Fucus* spp.'	Total
'Unclassified'	6.13	0.00	0.00	1.10
'Substratum'	**89.10**	5.79	0.97	18.20
'*Fucus* spp.'	4.02	**46.53**	5.82	17.31
'Asco_*Fucus* spp.'	0.74	47.68	**93.22**	63.38
Total	100	100	100	**100**

between *A. nodosum* and the other classes became more apparent at the canopy (Meddens et al., 2011), over individual frond scales (Kotta et al., 2014). The spectral similarity between 'Asco' and '*Fucus* spp.' Probably explains the small amount of misclassification between them. This was most evident towards the southern section of the site where a large area of '*Fucus* spp.' has been misclassified as 'Asco'. Visually this patch appeared significantly yellower and brighter than other '*Fucus* spp.' Areas, which may have led to confusion with the bright 'Asco' class. The remainder of the misclassification was spread throughout the site, highlighting some of the challenges when collecting training and reference data in spatially heterogeneous environments whereby polygons cannot necessarily account for small patches

TABLE 5 Aerial multispectral maximum-likelihood classifier (MLC) user accuracy (UA, probability of correct class assignment, calculated by dividing the number of correctly classified pixels by the total number of pixels in a class) and producer accuracy (PA, correctly classified reference pixels, calculated by dividing the number of correctly classified pixels by the total number of pixels that should be in a class) for each of the three cover classes computed using ENVI 5.4

Class	PA (%)	UA (%)	PA (pixels)	UA (pixels)
'Substratum'	89.10	87.96	1,439/1,615	1,439/1,636
'*Fucus* spp.'	46.53	78.02	1,214/2,609	1,214/1,556
'Asco_*Fucus* spp.'	93.22	77.95	4,440/4,763	4,440/5,696

of different classes within their boundaries (Foody, 2002). Spatial complexity could not be fully accounted for in the collection of training and reference data and this includes intraspecific variation, for example many of the 'Asco' pixels misclassified as '*Fucus* spp.' appeared to be in shaded areas behind, or between, boulders, which may have darkened their spectral response leading to misclassification (Wigmore, Mark, McKenzie, Baraer, & Lautz, 2019). The creation of specific shaded classes may help to resolve this in the future (Ishida et al., 2018) but given the present low classification error, it was not deemed necessary here.

As a result of the bands used by the Parrot Sequoia, the spectral similarity observed between 'Green' and '*Fucus* spp.' was to be

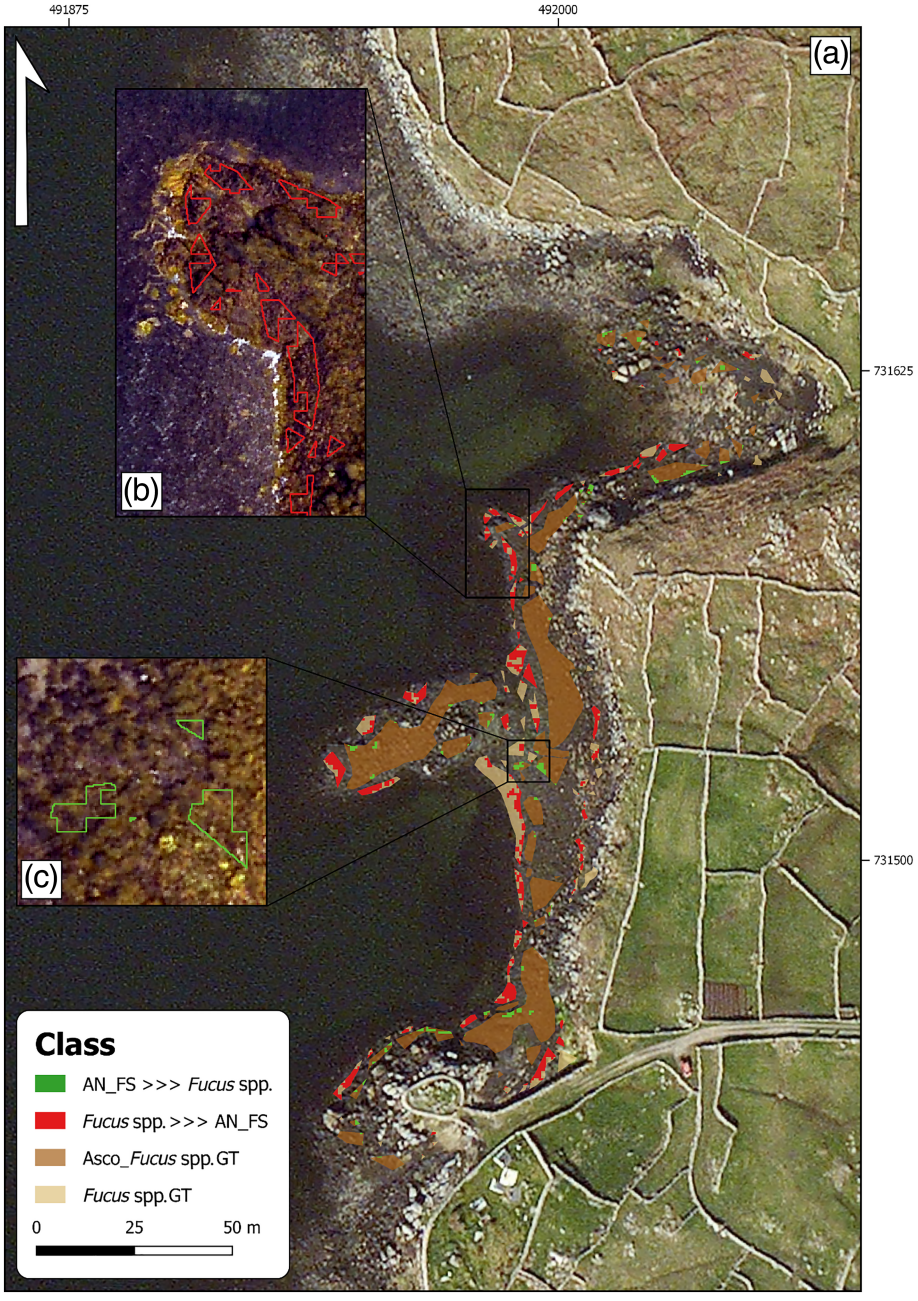

FIGURE 8 (a) Instances of misclassification between 'Asco_*Fucus* spp.' (labelled here as AN_FS) and '*Fucus* spp.' displayed above the respective ground-truth (GT) polygons for each class. Insets focus on notable misclassified areas where, in green, 'Asco_*Fucus* spp.' has been misclassified as '*Fucus* spp.' (c) and where, in red, the opposite occurs (b). Coordinates are in Irish Transverse Mercator (ITM)

expected. Previous research using spectral radiometers has highlighted the strong spectral separability between macroalgal groups (Casal, Kutser, Domínguez-Gómez, Sánchez-Carnero, & Freire, 2013; Kotta et al., 2014). Figure S3 shows that the spectrum of 'Green' was similar to that of both brown macroalgal classes, and with this sensor not having any bands below 550 nm, or between 550 and 660 nm, key distinguishing features of green macroalgae (single peak at 550 nm) and brown macroalgae (three peaks and troughs between 550 and 660 nm) (Kutser, Vahtmäe, & Metsamaa, 2006) were not recorded, potentially explaining the poor spectral separation. Ultimately, because of the small area covered by green macroalgal species, in comparison with other classes, its exclusion might not significantly alter the accuracy of the final classification.

4.2 | Aerial multispectral imagery

Although the classification results from the aerial multispectral imagery broadly agreed with the UAV imagery, managing to identify a belt dominated by *A. nodosum* ('Asco_*Fucus* spp.'), it was not able to identify a pure *A. nodosum* class. The resulting lower taxonomic resolution meant that it was not possible to determine an accurate area estimation for *A. nodosum* at the site. Coarser pixel sizes led to increased subpixel mixing of spectra, with one or more classes potentially being present within a single pixel (Lyons, Phinn, & Roelfsema, 2011; Su et al., 2006). The coarser resolution meant that it was difficult to accurately select enough training data for classes that cover a small area, such as 'Wrack', leading to its exclusion from the final classification. Such exclusions highlight the need for higher levels of spatial resolution, but also show that the decision of whether or not to include a class also depends on research objectives, and we chose to prioritize the classification accuracy for dominant cover classes over minor classes. Coarse pixel size was also responsible for the low spectral separability between 'Asco_*Fucus* spp.' and '*Fucus* spp.', where many pixels were spectrally heterogeneous (Belluco et al., 2006), containing mixtures of fucoid species that were not necessarily observable through visual analysis of the RGB imagery. The significant misclassification of '*Fucus* spp.' pixels as 'Asco_*Fucus* spp.' appears most prevalent across the boundary between the mid and lower intertidal zone, where there was a transition from an assemblage dominated by *A. nodosum* to an assemblage dominated by *Fucus* spp. (Figure 8). This highlights the difficulties in trying to distinguish between two spectrally similar classes.

4.3 | Satellite multispectral imagery

The spatial resolution of Sentinel-2 data was too coarse to allow for macroalgal species identification as the highest band resolutions (10 m) were still larger than the footprint covered by species present within the intertidal. The relatively coarse spatial resolution of some satellite imagery does not preclude its application for macroalgal monitoring, however. For species that form homogenous, monospecific stands, such as *Macrocystis pyrifera* off the coast of Santa Barbara, satellite imagery with 10-m resolution was able to provide accurate canopy cover estimations (Cavanaugh et al., 2010). If well supported by *in-situ* sampling (i.e. abundance and percentage cover), the ability of the satellite to identify the intertidal zone could allow for the broad extrapolation of localized *in-situ* biological data to regional-scale estimates of macroalgal extent. Yet, the time involved in conducting such detailed *in-situ* surveys would negate the efficiency provided by satellite remote sensing, and the resulting extent estimates will be significantly less accurate than those achieved through direct quantification of species extent using UAVs and aircraft.

4.4 | Effectiveness of high-resolution RGB data for training and reference data collection

The collection of accurate reference and training data directly impacts upon classification accuracy. When considering the future potential for large-scale intertidal macroalgal surveys it would be impractical (time and cost) to conduct extensive field campaigns. The potential for GPS (Laliberte & Rango, 2011) and image georeferencing errors (Jaud et al., 2018) would still create a bias towards selecting training and reference data from large homogenous stands of macroalgae (Foody, 2002), as observed when collecting data through the visual assessment of RGB imagery. UAVs can be used to efficiently collect training data over much larger areas than using field-based methods (Gray et al., 2018) and the accuracy of this method relies on achieving a high enough spatial resolution to enable complex patterns to be observed. The resolutions achieved by UAVs allow for the accurate and efficient collection of training and reference data through being able to accurately identify intertidal macroalgal species. The applicability may depend on the target species, however, but the distinctive morphological and colour properties of *A. nodosum* at the study site enhanced the accuracy of its identification.

4.5 | Operational considerations

From a spatial resolution perspective, this study has demonstrated how UAVs allow for the accurate classification and quantification of the distribution of *A. nodosum*. At present, such results are only likely to be achievable over small geographic areas because of current national UAV regulatory policies (Baena et al., 2018), despite battery technology allowing many UAVs to fly between 60 and 180 min. Although aircraft can cover much larger areas, they tend to have coarser spatial resolutions (Anderson & Gaston, 2013) that, depending on the research objectives, could reduce the classification accuracy, thereby limiting their usefulness for intertidal macroalgal resource assessment. The development and granting of 'beyond visual line of sight' (BVLOS) permission to companies and individuals who meet specified national aviation authority guidelines will allow the scaling up of UAV surveys to the point where they may offer a true mapping alternative to aircraft.

The cost-effectiveness of using remote sensing to map intertidal macroalgae will vary depending on the project requirements, with factors such as geographic scale potentially informing on the most suitable platform to use. Both the UAV and aerial surveys required similar work hours for data collection and processing, with the aerial survey able to collect data over a far larger geographic area. Hiring a company to conduct remote sensing surveys is the only feasible option for aerial surveys, yet for UAV surveys it may end up being more cost-effective, in the long term, to bring data collection and processing capabilities 'in-house', especially if temporal studies are planned. The only caveat of this approach is the initial set-up cost (i.e. UAV, GPS, sensor, software, and pilot training), the requirement for specialized technical knowledge, computing capabilities, and compliance with local regulations. Furthermore, the use of satellites may still prove a useful option depending on the research question. Higher spatial resolution satellites, such as RapidEye (5 m/pixel), may be applicable for studies looking at identifying and mapping broader taxonomic classification classes, such as macroalgal groups, over large areas (Brodie et al., 2018).

4.6 | Management implications of UAVs

At present, UAV technologies are well suited for the rapid, flexible, and cost-effective mapping of relatively small geographic areas and are well suited for the unique challenges of mapping the intertidal zone. Their capability to conduct multiple, repeat measurements (Manfreda et al., 2018) will also enhance their application in monitoring dynamic ecosystems, short-term events (algal blooms etc.), mobile fauna, and invasive species. Straightforward integration of multispectral sensors (e.g. DJI SkyPort) will further enhance applications for UAV technology, and technological and regulatory developments will only improve the ability of UAVs to contribute towards the establishment of accurate environmental baseline monitoring and will, in turn, inform resource conservation and management decisions (Connell et al., 2008). The world is changing and developments in drone regulatory policy, such as common EU regulations (https://www.easa.europa.eu/easa-and-you/civil-drones-rpas) together with a global move towards BVLOS operations, will present the possibility of long-range coastal macroalgal surveys in the not too distant future. This will improve the ability of interested stakeholders to efficiently manage and conserve intertidal macroalgal communities over large geographic areas. In addition to this, decreasing the costs of UAVs and sensors will make such technology accessible to a broader range of interested stakeholders, enabling a wide range of novel applications (Johnston, 2019).

Although the use of UAVs for monitoring macroalgal habitats is growing (Taddia et al., 2019; Tait et al., 2019), a range of different studies have incorporated UAVs into management and conservation research objectives. The monitoring of orangutans has been conducted using both RGB (Wich, Dellatore, Houghton, Ardi, & Koh, 2016) and thermal sensors (Burke et al., 2019), with the small size of UAVs making them ideal for operating in remote environments. UAVs have also proven capable of operating in challenging conditions, helping researchers to monitor the health (Pirotta et al., 2017) and physiology (Christiansen, Dujon, Sprogis, Arnould, & Bejder, 2016) of whales. Yet there remains a need for standardization in UAV monitoring protocols to account for variations caused by solar conditions, survey accuracy, and flight planning, to allow for direct comparisons of data between study sites and time (Assmann, Kerby, Cunliffe, & Myers-Smith, 2019).

5 | CONCLUSIONS

The probable increase of anthropogenic pressures upon intertidal macroalgal communities requires the development of accurate and efficient mapping methodologies to complement traditional field survey techniques and must also consider a range of different budgets. Different remote-sensing platforms each offer unique advantages and disadvantages, and their suitability for the mapping of intertidal macroalgal communities was compared. This study has demonstrated how UAV-mounted multispectral remote sensing was the most accurate of the three methods for assessing the distribution of *A. nodosum*, where having a high spatial resolution allowed complex spatial patterns to be observed. High-resolution RGB imagery facilitated the accurate collection of training and reference data, and this method is likely to complement the scaling up of UAV-based surveys in the future (Gray et al., 2018). The creation of sustainable resource management plans can now be underpinned by highly accurate, relatively low cost, and spatially comprehensive remote sensing data collection methodologies. The development of machine learning techniques is likely to yield improved classification results and has already proven useful for the automated identification of weeds within crop fields (de Castro et al., 2018; Gao, Nuyttens, Lootens, He, & Pieters, 2018).

Relatively inexpensive multispectral sensors, when mounted on a UAV, provide an effective macroalgal resource assessment tool when used in environments with low species diversity and homogenous cover of canopy-forming species. For repeat surveys, the most cost-effective solution is to bring data collection, processing, and analysis 'in-house', where decreasing technology costs, such as the 3dr Solo UAV (Johansen, Raharjo, & McCabe, 2018), are reducing financial barriers for those wishing to employ remote-sensing technology in their research: for example, enabling those in remote but biodiverse regions of the globe to better monitor and conserve their ecological resources (Vargas-Ramírez & Paneque-Gálvez, 2019). Lower costs and an increase in turnkey multispectral sensors may also facilitate the use of UAVs and multispectral sensors by local conservation charities and citizen science groups that, with the development of standardized mapping methodologies, could facilitate the accurate, high-resolution, monitoring of macroalgal resources over much wider spatial and temporal scales than is currently possible. Future work should explore potential seasonal and spatial trends in the accuracy of image capture and the implications for data processing. The likely variation in intra- and inter-specific spectral responses and relationships of intertidal macroalgae, often through seasonal variation in localized light regimes

(Stengel & Dring, 1998), may influence the ability of multispectral sensors to accurately discriminate between them.

ACKNOWLEDGEMENTS

The authors greatly appreciate the help provided by Fearghus Foyle, Aidan Magee, Daire Walsh, and Sean Mannion with the collection of the UAV and aerial imagery. We are also grateful for the assistance of Cole and the company of his dog, Sailor. This Cullen Fellowship research (grant-aid agreement no. CF/15/02) was funded by the Marine Institute under the Marine Research Sub-programme by the Irish Government and supported by INFOMAR (Integrated Mapping for the Sustainable Development of Ireland's Marine Resource).

ORCID

Thomas Rossiter https://orcid.org/0000-0002-6078-755X
Dagmar B. Stengel https://orcid.org/0000-0001-5871-9550

REFERENCES

Adão, T., Hruška, J., Pádua, L., Bessa, J., Peres, E., Morais, R., & Souza, J. (2017). Hyperspectreal Imaging: A Review of UAV-Based Sensors, Data Processing and Applications for Agriculture and Forestry. *Remote Sensing*, *9*, 1–30. https://doi.org/10.3390/rs9111110

Anderson, K., & Gaston, K. J. (2013). Lightweight unmanned aerial vehicles will revolutionize spatial ecology. *Frontiers in Ecology and the Environment*, *11*, 138–146. https://doi.org/10.1890/120150

Askari, M., McCarthy, T., Magee, A., & Murphy, D. (2019). Evaluation of grass quality under different soil management scenarios using remote sensing techniques. *Remote Sensing*, *11*, 1–23. https://doi.org/10.3390/rs11151835

Assmann, J. J., Kerby, J. T., Cunliffe, A. M., & Myers-Smith, I. H. (2019). Vegetation monitoring using multispectral sensors — best practices and lessons learned from high latitudes. *Journal of Unmanned Vehicle Systems*, *7*, 54–75. https://doi.org/10.1139/juvs-2018-0018

Baena, S., Boyd, D. S., & Moat, J. (2018). UAVs in pursuit of plant conservation - Real world experiences. *Ecological Informatics*, *47*, 2–9. https://doi.org/10.1016/j.ecoinf.2017.11.001

Bajjouk, T., Guillaumont, B., & Populus, J. (1996). Application of airborne imaging spectrometry system data to intertidal seaweed classification and mapping. *Hydrobiologia*, *326–327*, 463–471. https://doi.org/10.1007/BF00047847

Barrero, O., & Perdomo, S. A. (2018). RGB and multispectral UAV image fusion for Gramineae weed detection in rice fields. *Precision Agriculture*, *19*, 809–822. https://doi.org/10.1007/s11119-017-9558-x

Bell, T. W., Allen, J. G., Cavanaugh, K. C., & Siegel, D. A. (2020). Three decades of variability in California's giant kelp forests from the Landsat satellites. *Remote Sensing of Environment*, *238*, 1–13. https://doi.org/10.1016/j.rse.2018.06.039

Bell, T. W., Cavanaugh, K. C., & Siegel, D. A. (2015). Remote monitoring of giant kelp biomass and physiological condition: An evaluation of the potential for the Hyperspectral Infrared Imager (HyspIRI) mission. *Remote Sensing of Environment*, *167*, 218–228. https://doi.org/10.1016/j.rse.2015.05.003

Belluco, E., Camuffo, M., Ferrari, S., Modenese, L., Silvestri, S., Marani, A., & Marani, M. (2006). Mapping salt-marsh vegetation by multispectral and hyperspectral remote sensing. *Remote Sensing of Environment*, *105*, 54–67. https://doi.org/10.1016/j.rse.2006.06.006

Bentoutou, Y., Taleb, N., Kpalma, K., & Ronsin, J. (2005). An automatic image registration for applications in remote sensing. *IEEE Transactions on Geoscience and Remote Sensing*, *43*, 2127–2137. https://doi.org/10.1109/TGRS.2005.853187

Brodie, J., Ash, L. V., Tittley, I., & Yesson, C. (2018). A comparison of multispectral aerial and satellite imagery for mapping intertidal seaweed communities. *Aquatic Conservation: Marine and Freshwater Ecosystems*, *28*, 872–881. https://doi.org/10.1002/aqc.2905

Bruno, J. F., & Bertness, M. D. (2000). Habitat modification and facilitation in benthic marine communities. *Marine Community Ecology*. pp. 201–218. Retrieved from http://johnfbruno.web.unc.edu/files/2011/11/Bruno-Bertness-2001.pdf. (accessed: 30 July, 2019).

Burke, C., Rashman, M. F., Longmore, S. N., McAree, O., Glover-Kapfer, P., Ancrenaz, M., & Wich, S. A. (2019). Successful observation of orangutans in the wild with thermal-equipped drones. *Journal of Unmanned Vehicle Systems*, *7*, 235–257. https://doi.org/10.1139/juvs-2018-0035

Burns, P. D., Berns, R. S. & York, N. (1996). Analysis multispectral image capture. *The Fourth Color Imaging Conference: Color Science, Systems and Applications*, (November), 19–22. Retrieved from https://pdfs.semanticscholar.org/15ad/16c069efd2e313ec9edf0eda4ac19ed47bfe.pdf. (accessed: 18 October, 2019).

Candiago, S., Remondino, F., De Giglio, M., Dubbini, M., & Gattelli, M. (2015). Evaluating multispectral images and vegetation indices for precision farming applications from UAV Images. *Remote Sensing*, *7*, 4026–4047. https://doi.org/10.3390/rs70404026

Carrasco-Escobar, G., Manrique, E., Ruiz-Cabrejos, J., Saavedra, M., Alava, F., Bickersmith, S., … Gamboa, D. (2019). High-accuracy detection of malaria vector larval habitats using drone-based multispectral imagery. *PLoS Neglected Tropical Diseases*, *13*, 1–24. https://doi.org/10.1371/journal.pntd.0007105

Casal, G., Kutser, T., Domínguez-Gómez, J. A., Sánchez-Carnero, N., & Freire, J. (2013). Assessment of the hyperspectral sensor CASI-2 for macroalgal discrimination on the Ría de Vigo coast (NW Spain) using field spectroscopy and modelled spectral libraries. *Continental Shelf Research*, *55*, 129–140. https://doi.org/10.1016/j.csr.2013.01.010

Casal, G., Sánchez-Carnero, N., Domínguez-Gómez, J. A., Kutser, T., & Freire, J. (2012). Assessment of AHS (Airborne Hyperspectral Scanner) sensor to map macroalgal communities on the Ría de vigo and Ría de Aldán coast (NW Spain). *Marine Biology*, *159*, 1997–2013. https://doi.org/10.1007/s00227-012-1987-5

Casal, G., Sánchez-Carnero, N., Sánchez-Rodríguez, E., & Freire, J. (2011). Remote sensing with SPOT-4 for mapping kelp forests in turbid waters on the south European Atlantic shelf. *Estuarine, Coastal and Shelf Science*, *91*, 371–378. https://doi.org/10.1016/j.ecss.2010.10.024

Cavanaugh, K. C., Siegel, D. A., Kinlan, B. P., & Reed, D. C. (2010). Scaling giant kelp field measurements to regional scales using satellite observations. *Marine Ecology Progress Series*, *403*, 13–27. https://doi.org/10.3354/meps08467

Christiansen, F., Dujon, A. M., Sprogis, K. R., Arnould, J. P. Y., & Bejder, L. (2016). Noninvasive unmanned aerial vehicle provides estimates of the energetic cost of reproduction in humpback whales. *Ecosphere*, *7*, 1–18. https://doi.org/10.1002/ecs2.1468

Clevers, J. G. P. W., & Gitelson, A. A. (2013). Remote estimation of crop and grass chlorophyll and nitrogen content using red-edge bands on sentinel-2 and-3. *International Journal of Applied Earth Observation and Geoinformation*, *23*, 344–351. https://doi.org/10.1016/j.jag.2012.10.008

Colefax, A. P., Butcher, P. A., & Kelaher, B. P. (2018). The potential for unmanned aerial vehicles (UAVs) to conduct marine fauna surveys in place of manned aircraft. *ICES Journal of Marine Science*, *75*, 1–8. https://doi.org/10.1093/icesjms/fsx100

Colomina, I., & Molina, P. (2014). Unmanned aerial systems for photogrammetry and remote sensing: A review. *ISPRS Journal of Photogrammetry and Remote Sensing*, *92*, 79–97. https://doi.org/10.1016/j.isprsjprs.2014.02.013

Connell, S., Turner, D., Shepherd, S., Miller, D., Russell, B., Kildea, T., … Cheshire, A. (2008). Recovering a lost baseline: missing kelp forests from a metropolitan coast. *Marine Ecology Progress Series*, *360*, 63–72. https://doi.org/10.3354/meps07526

Cruzan, M. B., Weinstein, B. G., Grasty, M. R., Kohrn, B. F., Hendrickson, E. C., Arredondo, T. M., & Thompson, P. G. (2016). Small unmanned aerial vehicles (Micro-UAVs, drones) in plant ecology. *Applications in Plant Sciences*, *4*, 1–11. https://doi.org/10.3732/apps.1600041

Dash, J. P., Pearse, G. D., & Watt, M. S. (2018). UAV multispectral imagery can complement satellite data for monitoring forest health. *Remote Sensing*, *10*, 1–22. https://doi.org/10.3390/rs10081216

Davies, A. J., Johnson, M. P., & Maggs, C. A. (2007). Limpet grazing and loss of *Ascophyllum nodosum* canopies on decadal time scales. *Marine Ecology Progress Series*, *339*, 131–141. https://doi.org/10.3354/meps339131

de Castro, A., Torres-Sánchez, J., Peña, J., Jiménez-Brenes, F., Csillik, O., & López-Granados, F. (2018). An automatic random forest-OBIA algorithm for early weed mapping between and within crop rows using UAV imagery. *Remote Sensing*, *10*, 1–11. https://doi.org/10.3390/rs10020285

Dekker, A. G., Byrne, G. T., Brando, V. E. & Anstee, J. M. (2003). Hyperspectral mapping of intertidal rock platform vegetation as a tool for adaptive management. *CSIRO*. 1–76. Retrieved from http://www.clw.csiro.au/publications/technical2003/tr9-03.pdf. (accessed 30 July, 2019).

Dierssen, H. M., Chlus, A., & Russell, B. (2015). Hyperspectral discrimination of floating mats of seagrass wrack and the macroalgae Sargassum in coastal waters of Greater Florida Bay using airborne remote sensing. *Remote Sensing of Environment*, *167*, 247–258. https://doi.org/10.1016/j.rse.2015.01.027

Doughty, C., & Cavanaugh, K. (2019). Mapping coastal wetland biomass from high resolution Unmanned Aerial Vehicle (UAV) imagery. *Remote Sensing*, *11*, 1–16. https://doi.org/10.3390/rs11050540

Duffy, J. P., Pratt, L., Anderson, K., Land, P. E., & Shutler, J. D. (2017). Spatial assessment of intertidal seagrass meadows using optical imaging systems and a lightweight drone. *Estuarine, Coastal and Shelf Science*, *200*, 169–180. https://doi.org/10.1016/j.ecss.2017.11.001

Foody, G. M. (2002). Status of land cover classification accuracy assessment. *Remote Sensing of Environment*, *80*, 185–201. https://doi.org/10.1016/S0034-257(01)00295-4

Foody, G. M., Campbell, N. A., Trodd, N. M., & Wood, T. F. (1992). Derivation and applications of probabilistic measures of class membership from the maximum-likelihood classification. *Photogrammetric Engineering and Remote Sensing*, *58*, 1335–1341. Retrieved from https://www.asprs.org/wp-content/uploads/pers/1992journal/sep/1992_sep_1335-1341.pdf. (accessed 30 July, 2019).

Gao, J., Nuyttens, D., Lootens, P., He, Y., & Pieters, J. G. (2018). Recognising weeds in a maize crop using a random forest machine-learning algorithm and near-infrared snapshot mosaic hyperspectral imagery. *Biosystems Engineering*, *170*, 39–50. https://doi.org/10.1016/j.biosystemseng.2018.03.006

Garono, R. J., Simenstad, C. A., Robinson, R., & Ripley, H. (2004). Using high spatial resolution hyperspectral imagery to map intertidal habitat structure in Hood Canal, Washington, U.S.A. *Canadian Journal of Remote Sensing*, *30*, 54–63. https://doi.org/10.5589/m03-052

Gray, P. C., Ridge, J. T., Poulin, S. K., Seymour, A. C., Schwantes, A. M., Swenson, J. J., & Johnston, D. (2018). Integrating drone imagery into high resolution satellite remote sensing assessments of estuarine environments. *Remote Sensing*, *10*. 1–24. https://doi.org/10.3390/rs10081257

Hennig, B. D., Cogan, C. B., & Bartsch, I. (2007). Hyperspectral remote sensing and analysis of intertidal zones: A contribution to monitor coastal biodiversity. *Proceedings of the First Geoinformatics Forum Salzburg*, *2007*, 62–73. Retrieved from http://epic.awi.de/Publications/Hen2007c.pdf. (accessed: 30 July, 2019).

Ishida, T., Kurihara, J., Viray, F. A., Namuco, S. B., Paringit, E. C., Perez, G. J., … Marciano, J. J. (2018). A novel approach for vegetation classification using UAV-based hyperspectral imaging. *Computers and Electronics in Agriculture*, *144*, 80–85. https://doi.org/10.1016/j.compag.2017.11.027

Jacobsen, A., Nielsen, A. A., Ejrnaes, R., & Groom, G. B. (1999). Spectral identification of Danish grassland classes related to management and plant species composition. *Proceedings of 4th International Airborne Remote Sensing Conference and Exhibition/21st Canadian Symposium on Remote Sensing*, *1*, 74–81. Retrieved from http://www.neri.dk/1_Viden/2_Publikationer/3_Ovrige/rapporter/Artikel3_anne_LAND.pdf. (accessed: 18 October, 2019).

Jaud, M., Le Dantec, N., Ammann, J., Grandjean, P., Constantin, D., Akhtman, Y., … Merminod, B. (2018). Direct georeferencing of a push-broom, lightweight hyperspectral system for mini-UAV applications. *Remote Sensing*, *10*, 1–15. https://doi.org/10.3390/rs10020204

Jensen, A. M., Hardy, T., McKee, M. & Chen, Y. Q. (2011). Using a multispectral autonomous unmanned aerial remote sensing platform (AggieAir) for riparian and wetlands applications. *International Geoscience and Remote Sensing Symposium (IGARSS)*, 3413–3416. https://doi.org/10.1109/IGARSS.2011.6049953

Jia, X., & Richards, J. A. (1994). Efficient Maximum Likelihood Classification for imaging spectrometer data sets. *IEEE Transactions on Geoscience and Remote Sensing*, *32*, 274–281. https://doi.org/10.1109/36.295042

Johansen, K., Raharjo, T., & McCabe, M. F. (2018). Using multi-spectral UAV imagery to extract tree crop structural properties and assess pruning effects. *Remote Sensing*, *10*, 1–21. https://doi.org/10.3390/rs10060854

Johnston, D. W. (2019). Unoccupied aircraft systems in marine science and conservation. *Annual Review of Marine Science*, *11*, 439–463. https://doi.org/10.1146/annurev-marine-010318-095323

Kazantsev, T., Samberg, A., Ametov, F., Shevchenko, V., Bondarenko, O., Furier, M., et al. (2018). COTS UAV-borne multispectral system for vegetation monitoring. In C. M. Neale, & A. Maltese (Eds.), *Remote sensing for agriculture, ecosystems, and hydrology XX (p. 12)*. Berlin: SPIE. https://doi.org/10.1117/12.2501859

Kerr, J. T., & Ostrovsky, M. (2003). From space to species: Ecological applications for remote sensing. *Trends in Ecology & Evolution*, *18*, 299–305. https://doi.org/10.1016/S0169-5347(03)00071-5

Könnecker, G., & Keegan, B. (1983). Littoral and benthic investigations on the west coast of Ireland: XVII. The epibenthic animal associations of Kilkieran Bay. *Proceedings of the Royal Irish Academy, Section B: Biological, Geological, and Chemical Science*, *83B*, 309–324. https://www.jstor.org/stable/20494425

Kotta, J., Remm, K., Vahtmäe, E., Kutser, T., & Orav-Kotta, H. (2014). In-air spectral signatures of the Baltic Sea macrophytes and their statistical separability. *Journal of Applied Remote Sensing*, *8*, 1–14. https://doi.org/10.1117/1.JRS.8.083634

Kutser, T., Vahtmäe, E., & Metsamaa, L. (2006). Spectral library of macroalgae and benthic substrates in Estonian coastal waters. *Proceedings of the Estonian Academy of Science, Biology and Ecology*, *55*, 329–340. Retrieved from http://www.kirj.ee/public/va_bo/bio-2006-4-5.pdf. (accessed: 30 July, 2019).

Laliberte, A. S., & Rango, A. (2011). Image processing and classification procedures for analysis of sub-decimeter imagery acquired with an unmanned aircraft over arid rangelands. *GIScience and Remote Sensing*, *48*, 4–23. https://doi.org/10.2747/1548-1603.48.1.4

Lechner, A. M., Fletcher, A., Johansen, K., & Erskine, P. (2012). Characterising upland swamps using object-based classification methods and hyper-spatial resolution imagery derived from an Unmanned Aerial Vehicle. *ISPRS Annals of the Photogrammetry, Remote*

Sensing and Spatial Information Sciences, *1*, 101–106. https://doi.org/10.5194/isprsannals-I-4-101-2012

Lyons, M., Phinn, S., & Roelfsema, C. (2011). Integrating Quickbird multi-spectral satellite and field data: Mapping bathymetry, seagrass cover, seagrass species and change in Moreton Bay, Australia in 2004 and 2007. *Remote Sensing*, *3*, 42–64. https://doi.org/10.3390/rs3010042

Manfreda, S., McCabe, M., Miller, P., Lucas, R., Pajuelo Madrigal, V., Mallinis, G., et al. (2018). On the use of unmanned aerial systems for environmental monitoring. *Remote Sensing*, *10*, 1–28. https://doi.org/10.3390/rs10040641

Marshall, M., & Thenkabail, P. (2015). Advantage of hyperspectral EO-1 Hyperion over multispectral IKONOS, GeoEye-1, WorldView-2, Landsat ETM+, and MODIS vegetation indices in crop biomass estimation. *ISPRS Journal of Photogrammetry and Remote Sensing*, *108*, 205–218. https://doi.org/10.1016/j.isprsjprs.2015.08.001

Matese, A., Toscano, P., Di Gennaro, S. F., Genesio, L., Vaccari, F. P., Primicerio, J., … Gioli, B. (2015). Intercomparison of UAV, Aircraft and Satellite Remote Sensing Platforms for Precision Viticulture. *Remote Sensing*, *7*, 2971–2990. https://doi.org/10.3390/rs70302971

McDermid, G., Franklin, S., & LeDrew, E. (2005). Remote Sensing for large area multi-jurisdictional habitat mapping. *Progress in Physical Geography*, *4*, 449–474. https://doi.org/10.1191/0309133305pp455ra

McFeeters, S. K. (1996). The use of the Normalized Difference Water Index (NDWI) in the delineation of open water features. *International Journal of Remote Sensing*, *17*, 1425–1432. https://doi.org/10.1080/01431169608948714

McRoberts, R. E., Stehman, S. V., Liknes, G. C., Næsset, E., Sannier, C., & Walters, B. F. (2018). The effects of imperfect reference data on remote sensing-assisted estimators of land cover class proportions. *ISPRS Journal of Photogrammetry and Remote Sensing*, *142*, 292–300. https://doi.org/10.1016/j.isprsjprs.2018.06.002

Meddens, A. J. H., Hicke, J. A., & Vierling, L. A. (2011). Evaluating the potential of multispectral imagery to map multiple stages of tree mortality. *Remote Sensing of Environment*, *115*, 1632–1642. https://doi.org/10.1016/j.rse.2011.02.018

Mineur, F., Arenas, F., Assis, J., Davies, A. J., Engelen, A. H., Fernandes, F., … de Clerck, O. (2015). European seaweeds under pressure: Consequences for communities and ecosystem functioning. *Journal of Sea Research*, *98*, 91–108. https://doi.org/10.1016/j.seares.2014.11.004

Murfitt, S. L., Allan, B. M., Bellgrove, A., Rattray, A., Young, M. A., & Ierodiaconou, D. (2017). Applications of unmanned aerial vehicles in intertidal reef monitoring. *Scientific Reports*, *7*, 1–11. https://doi.org/10.1038/s41598-017-10818-9

National Parks and Wildlife Service (NPWS). (2014). Kilkieran Bay and Islands SAC (site code 2111) Conservation objectives supporting document - coastal habitats https://www.npws.ie/sites/default/files/publications/pdf/002111%20Kilkieran%20Bay%20and%20Islands%20SAC%20Coastal%20Supporting%20Doc%20V1.pdf. (accessed 24 July, 2019).

Oppelt, N., Schulze, F., Bartsch, I., Doernhoefer, K., & Eisenhardt, I. (2012). Hyperspectral classification approaches for intertidal macroalgae habitat mapping: A case study in Heligoland. *Optical Engineering*, *51*, 1–11. https://doi.org/10.1117/1.OE.51.11.111703

Paola, J. D., & Schowengerdt, R. A. (1995). A detailed comparison of backpropagation neural network and maximum-likelihood classifiers for urban land use classification. *IEEE Transactions on Geoscience and Remote Sensing*, *33*, 981–996. https://doi.org/10.1109/36.406684

Pe'eri, S., Morrison, J. R., Short, F., Mathieson, A., Brook, A. & Trowbridge, P. (2008). Macroalgae and eelgrass mapping in Great Bay Estuary using AISA hyperspectral imagery. *A Final Report to The New Hampshire Estuaries Project*, *1*, p. 148 Retrieved from http://www.prep.unh.edu/resources/pdf/macroalgae_and_eelgrass-unh-09.pdf. (accessed: 30 July, 2019).

Petropoulos, G. P., Vadrevu, K. P., Xanthopoulos, G., Karantounias, G., & Scholze, M. (2010). A comparison of spectral angle mapper and artificial neural network classifiers combined with landsat TM imagery analysis for obtaining burnt area mapping. *Sensors*, *10*, 1967–1985. https://doi.org/10.3390/s100301967

Pirotta, V., Smith, A., Ostrowski, M., Russell, D., Jonsen, I. D., Grech, A., & Harcourt, R. (2017). An economical custom-built drone for assessing whale health. *Frontiers in Marine Science*, *4*, 1–12. https://doi.org/10.3389/fmars.2017.00425

Richards, J. A. & Jia, X. (2006). Remote Sensing Digital Image Analysis. New York. https://doi.org/10.1016/S0169-555X(01)00164-7

Sides, E. M., Picton, B. E., Emblow, C. S., Morrow, C. C. & Costello, M. J. (1994). *Marine commmunities of Kilkieran Bay, the Aran Islands and the Skerd Rocks and an assessment of their conservation importance*. Trinity College, Dublin. https://www.npws.ie/sites/default/files/publications/pdf/Sides_et_al_1994_Kilkieran_Bay.pdf. (accessed 25 July, 2019).

Smith, G., & Milton, E. (1999). The use of the empirical line method to calibrate remotely sensed data to reflectance. *International Journal of Remote Sensing*, *20*, 2653–2662. https://doi.org/10.1080/014311699211994

Stekoll, M. S., Deysher, L. E., & Hess, M. (2006). A remote sensing approach to estimating harvestable kelp biomass. *Journal of Applied Phycology*, *18*, 323–334. https://doi.org/10.1007/s10811-006-9029-7

Stengel, D. B., & Dring, M. J. (1997). Morphology and *in situ* growth rates of plants of *Ascophyllum nodosum* (Phaeophyta) from different shore levels and responses of plants to vertical transplantation. *European Journal of Phycology*, *32*, 193–202. https://doi.org/10.1017/S0967026297001200

Stengel, D. B., & Dring, M. J. (1998). Seasonal variation in the pigment content and photosynthesis of different thallus regions of *Ascophyllum nodosum* (Fucales, Phaeophyta) in relation to position in the canopy. *Phycologia*, *37*, 259–268. https://doi.org/10.2216/i0031-8884-37-4-259.1

Su, H., Karna, D., Fraim, E., Fitzgerald, M., Dominguez, R., Myers, J. S., … Mace, T. (2006). Evaluation of eelgrass beds mapping using a high-resolution airborne multispectral scanner. *Photogrammetric Engineering and Remote Sensing*, *72*, 789–797. https://doi.org/10.14358/PERS.72.7.789

Taddia, Y., Russo, P., Lovo, S., & Pellegrinelli, A. (2019). Multispectral UAV monitoring of submerged seaweed in shallow water. *Applied Geomatics*, 1–16. https://doi.org/10.1007/s12518-019-00270-x

Tait, L., Bind, J., Charan-Dixon, H., Hawes, I., Pirker, J., & Schiel, D. (2019). Unmanned Aerial Vehicles (UAVs) for monitoring macroalgal biodiversity: Comparison of RGB and multispectral imaging sensors for biodiversity assessments. *Remote Sensing*, *11*, 1–18. https://doi.org/10.3390/rs11192332

Vadas, R. L. Sr., Wright, W. A., & Beal, B. F. (2004). Biomass and productivity of intertidal rockweeds (*Ascophyllum nodosum* LeJolis) in Cobscook Bay. *Northeastern Naturalist*, *11*, 123–142. https://www.jstor.org/stable/60225652

van Iersel, W., Straatsma, M., Middelkoop, H., & Addink, E. (2018). Multitemporal Classification of River Floodplain Vegetation Using Time Series of UAV Images. *Remote Sensing*, *10*, 1–18. https://doi.org/10.9330/rs10071144

Vargas-Ramírez, N., & Paneque-Gálvez, J. (2019). The global emergence of community drones (2012–2017). *Drones*, *3*, 1–24. https://doi.org/10.3390/drones3040076

Ventura, D., Bonifazi, A., Gravina, M. F., Belluscio, A., & Ardizzone, G. (2018). Mapping and classification of ecologically sensitive marine habitats using unmanned aerial vehicle (UAV) imagery and object-based image analysis (OBIA). *Remote Sensing*, *10*, 1–23. https://doi.org/10.3390/rs10091331

Wich, S., Dellatore, D., Houghton, M., Ardi, R., & Koh, L. P. (2016). A preliminary assessment of using conservation drones for Sumatran orang-

utan (*Pongo abelii*) distribution and density. *Journal of Unmanned Vehicle Systems*, *4*, 45–52. https://doi.org/10.1139/juvs-2015-0015

Wigmore, O., Mark, B., McKenzie, J., Baraer, M., & Lautz, L. (2019). Sub-metre mapping of surface soil moisture in proglacial valleys of the tropical Andes using a multispectral unmanned aerial vehicle. *Remote Sensing of Environment*, *222*, 104–118. https://doi.org/10.1016/j.rse.2018.12.024

Xu, H. (2006). Modification of normalised difference water index (NDWI) to enhance open water features in remotely sensed imagery. *International Journal of Remote Sensing*, *27*, 3025–3033. https://doi.org/10.1080/01431160600589179

SUPPORTING INFORMATION

Additional supporting information may be found online in the Supporting Information section at the end of this article.

How to cite this article: Rossiter T, Furey T, McCarthy T, Stengel DB. Application of multiplatform, multispectral remote sensors for mapping intertidal macroalgae: A comparative approach. *Aquatic Conserv: Mar Freshw Ecosyst*. 2020;30:1595–1612. https://doi.org/10.1002/aqc.3357